CHAPTER 13

Microfabricated Silicone Elastomeric Post Arrays for Measuring Traction Forces of Adherent Cells

Nathan J. Sniadecki* **and Christopher S. Chen*,†**

*Department of Bioengineering
University of Pennsylvania
Philadelphia, Pennsylvania 19104

†Department of Physiology
University of Pennsylvania
Philadelphia, Pennsylvania 19104

Abstract
I. Introduction
II. Microfabrication of the Micropost Arrays
  A. Standard Photolithography
  B. SU-8 Photolithography for Micropost Arrays
  C. Soft Lithography
  D. Troubleshooting and Helpful Suggestions
III. Characterization of Micropost Spring Constant
  A. Beam-Bending Theory
  B. Measurement of Micropost Stiffness
IV. Analysis of Traction Forces Through Micropost Deflections
  A. Substrate Preparation
  B. Staining and Microscopy of Micropost Arrays
  C. Image Analysis Techniques
V. Experimental Applications of Microposts and Discussion
References

METHODS IN CELL BIOLOGY, VOL. 83
Copyright 2007, Elsevier Inc. All rights reserved.

0091-679X/07 $35.00
DOI: 10.1016/S0091-679X(07)83013-5

Abstract

Nonmuscle cells exert biomechanical forces known as traction forces on the extracellular matrix (ECM). Spatial coordination of these traction forces against the ECM is in part responsible for directing cell migration, for remodeling the surrounding tissue scaffold, and for the folds and rearrangements seen during morphogenesis. The traction forces are applied through a number of discrete adhesions between a cell and the ECM. We have developed a device consisting of an array of flexible, microfabricated posts capable of measuring these forces under an adherent cell. Functionalizing the top of each post with ECM protein allows cells to attach and spread across the tops of the posts. Deflection of the tips of the posts is proportional to cell-generated traction forces during cell migration or contraction. In this chapter, we describe the microfabrication, preparation, and experimental use of such microfabricated post array detector system (mPADs).

I. Introduction

Aside from bursts of locomotion during embryonic development or wound healing, most nonphagocytic cells in tissues lead a relatively nonmotile existence. Yet, underlying this apparently stationary state, cells can generate biomechanical forces that are important for cytokinesis (Scholey *et al.*, 2003), cortical contraction (Adelstein, 1982), cytoskeletal rearrangement (Ingber, 1993, 2003), adhesion remodeling (Geiger *et al.*, 2001), and sensing the elasticity of the microenvironment (Discher *et al.*, 2005). Cells generate force through fibrous bundles of myosin acting on actin microfilaments in the cytoskeleton (Huxley, 2004). In muscle cells, the actin–myosin bundles are known as myofibrils, while in nonmuscle cells, they are known as stress fibers. Myosin moves in a stepwise, walking cycle along actin microfilaments. During each power stroke, it exerts pulling forces of 3–4 pN on actin filaments of opposite polarities to shorten the total length of the fibrous bundle (Brenner, 2006; Finer *et al.*, 1994). The ends of many of these microfilaments are linked to focal adhesions (FAs), which are transmembrane "spot-welds" that attach cells to the extracellular matrix (ECM) through integrin receptors (Chapter 5 by Spatz and Geiger, this volume) or to adherens junctions (AJs), which are intercellular patches of cadherins that hold cells together (Fig. 1A). Contraction of the actin–myosin bundle thus leads to the exertion of concentrated stress at these loci of attachment. At FAs, stress acts on the matrix lattice and creates "traction forces" to propel a cell forward, to induce strain in the matrix fibers (e.g., collagen), and perhaps to remodel the matrix. Measuring traction forces generated by cells can thus provide insight into how intracellular forces regulate and are regulated by other cell functions.

Several techniques have been developed to measure these forces and biochemical activities associated with them. Traction forces of locomotive fibroblasts and other cell types were first observed as wrinkles in a thin, flexible film of silicone rubber (Harris *et al.*, 1980). The numbers and lengths of wrinkles or buckles gave a rough gauge of traction forces. This simple yet elegant tool provided insights into

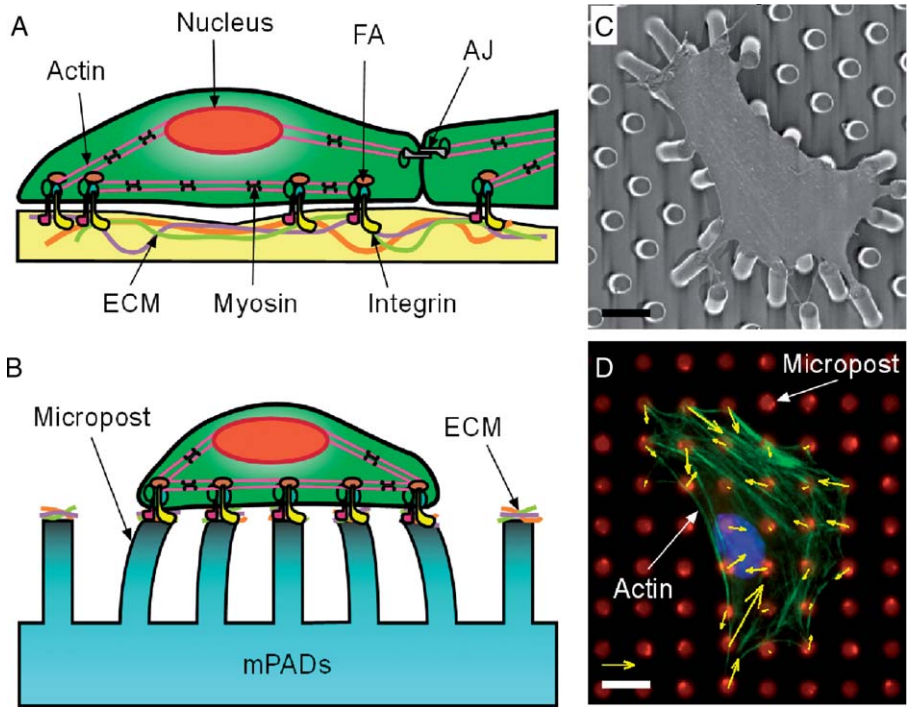

Fig. 1 Measurement of traction forces with microfabricated post array detector system (mPADs). (A) Myosin-driven sliding of actin microfilaments (stress fibers) causes forces to be loaded at focal adhesions (FAs), which attach the cell to the ECM through integrin receptors and at adherens junctions (AJs), which mediate cell–cell adhesions. (B) Forces at FAs, known as traction forces, are measured with the mPADs through the deflection of individual microposts. (C) Electron micrograph of a cell attached to the top of the microposts. Scale bar, 10 μm. (D) Vector map of traction forces is obtained by measuring the deflection of each micropost (DiI) due to the contraction of actin microfilament bundles (Phalloidin-Alex Fluor 488) within a cell (nucleus, Hoescht 33258). Scale bar, 10 μm; arrow, 20 nN.

the molecular pathways that regulated traction forces, stress fiber formation, and FA assembly (Chrzanowska-Wodnicka and Burridge, 1996; Helfman *et al.*, 1999). To better assess film distortions and allow measurements of traction forces, small latex beads were embedded into nonwrinkling silicone films for the quantification of film distortion during cell migration (Lee *et al.*, 1994). Subsequently, fluorescent microbeads were embedded into polyacrylamide gels, which could be cross-linked to different degrees in order to "tune" the stiffness of the elastic substrate for the range of traction forces generated by a particular cell type (Dembo and Wang, 1999). Arrays of fluorescent beads imprinted onto elastomeric substrates afforded even great precision than randomly seeded beads for the measurement of traction forces at individual FAs (Balaban *et al.*, 2001). Additionally, microfabricated cantilevers that deflect parallel to the plane of cell migration have provided measurements of transient tractions forces underneath small areas of a migrating cell (Galbraith and Sheetz, 1997): as a cell migrated over each microcantilever, the cantilever's deflection allowed a simple calculation of the local traction force.

To expand on this general approach, we have developed a microfabricated system that uses an array of vertical cantilevers to measure the traction forces at multiple locations on a cell (Tan *et al.*, 2003; Fig. 1B and C). During migration or contraction of a cell, its traction forces bend several posts such that each tip deflection is linearly proportional to the local force (Fig. 1D). However, while this technique can be straightforward to trained engineers, it requires many techniques that may not be familiar to a typical cell biologist. The goal of this chapter is to describe these techniques in sufficient detail such that they can be reproduced reliably and with minimal outside resources. In this chapter, we will describe (1) the fabrication steps used to construct the microfabricated post array detector system (mPADs), (2) the methods used to calibrate micropost stiffness, (3) the modification of mPADs for cell attachment, (4) the techniques in microscopy and image analysis for measuring micropost deflections, and (5) some applications with the mPADs for understanding cell mechanics.

II. Microfabrication of the Micropost Arrays

The mPADs are composed of a transparent silicone rubber called polydimethylsiloxane (PDMS), which can be modified with different surface treatments to allow or prevent deposition of ECM proteins onto the posts. Each micropost is cylindrical in shape, and the diameters (D), spacing (S), and heights (L) within an array are kept strictly uniform (within a fraction of a micrometer) in order to accurately measure traction forces ($D = 3\ \mu$m, $S = 6$–$9\ \mu$m, and $L = 8$–$12\ \mu$m, respectively). Due to the microscale dimensions of the microposts, it is necessary to fabricate the devices with techniques developed in the semiconductor industry for the fabrication of integrated circuits (ICs) and microelectrical mechanical systems (MEMS). The first step involves photolithography of a hard master made from the photoresist SU-8. The second step consists of molding the master in PDMS to create soft replicas of the arrays of microposts.

The master can be fabricated as either a positive or a negative replica of the micropost arrays—positive being microposts of SU-8 and negative being holes within a film of SU-8. For a positive master, two casting steps in PDMS are required to generate the PDMS mPADs (Fig. 2). The first casting generates a negative mold, into which PDMS is cast a second time to create the array of microposts. With this process, multiple molds can be made in batch from the same SU-8 master. For a negative master, PDMS is directly cast onto the master to form the final product. This process eliminates one step from the positive master approach, but with a drawback that PDMS tends to get clogged into the SU-8 holes, which can lead to degradation of a negative master. In our laboratory, we have chosen to fabricate arrays of microposts with a positive master and we describe this technique here. In discussing the fabrication, we first provide a general introduction to photolithography, then detail the steps specific to fabricating the mPAD master in SU-8, and finally describe the replication process in PDMS.

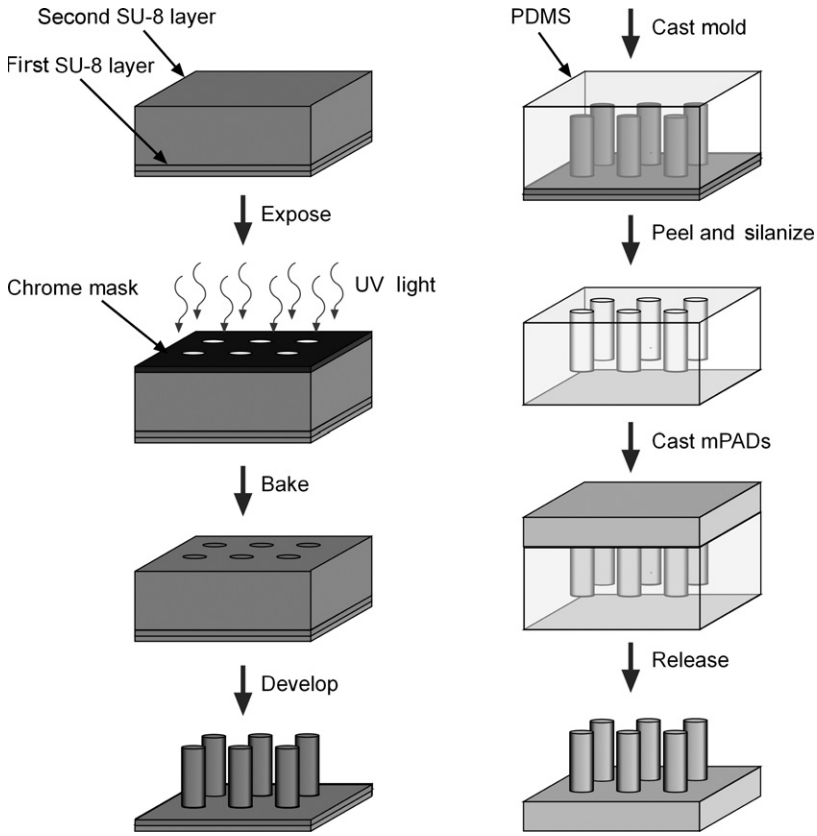

Fig. 2 Steps involved in the fabrication of mPADs. The process involves two photolithography steps of the SU-8 film and two soft lithography steps with PDMS.

A. Standard Photolithography

While we present below a concise introduction to the technique of photolithography as it pertains to fabricating mPADs, there are several excellent sources that describe this process in greater detail (Campbell, 2001; Jaeger, 2002; Madou, 1997). Standard photolithography involves the exposure of photosensitive material through a photomask. In MEMS or IC fabrication, the photosensitive material is photoresist such as SU-8, which is a polymer that can be patterned depending on where transparent patterns on the photomask allow light to pass through. In the case of positive photoresist, ultraviolet (UV) light causes scission in the polymer, rendering it more soluble in the high-pH developer solution than the unexposed regions. For negative photoresist such as SU-8, UV light enables cross-linking of the polymer in the exposed region, making it insoluble to the organic developer.

Each commercially available resist has its own recommended steps to follow in its use, but a general procedure is as follows. First, photoresist polymer is poured

onto a wafer and—in order to generate a film of uniform thickness on the wafer—the wafer is spun at 1000–4000 rpm using a photoresist spin coater, which is a centrifuge-like device with a vacuum chuck and adjustable rotational speed to allow control of the uniformity and thickness of the film. The polymer film on the wafer is "soft baked" between 90 and 100°C to evaporate out solvent from the polymer film. The wafer is then overlaid with the photomask in an exposure system, commonly known as a mask aligner, in order to correctly position the patterns to the wafer. After exposure according to the manufacturer's specification, the wafer is placed into a developer solution to wash away the soluble regions, leaving behind the insoluble patterns in the photoresist. Expertise with spin coaters, mask aligners, and photolithography is often available within electrical engineering and material science departments, or in a core microfabrication facility at many universities.

Photomasks contain microscopic features that are designed like blueprints with a computer-aided design (CAD) tool. A photomask consists of a soda lime glass or quartz plate with a patterned chromium layer, which absorbs visible to deep UV light and casts shadows of designed pattern on the photoresist. For feature sizes as small as 1–2 μm, such masks can be readily obtained from commercial outsourcing services or at local university facilities. The patterns on the chrome mask are "written" using optical pattern generators or e-beam mask writers. Once a design is laid out and fabricated, a single mask can be used repeatedly to generate the same pattern on tens of thousands of silicon wafers.

A less expensive approach but with a trade-off of larger feature sizes and lower resolution is a film photomask. Here, a transparency film is printed with minimum feature sizes of 10–20 μm using a high-resolution laser printer or photoplotter that is often available at custom print shops (graphic printing or reprography). The film is fixed to a glass plate with clear tape along the edges and shadows the photoresist like the metal layer of a chrome mask. A film mask is not sufficient for generating the mPADs master because 1- to 3-μm feature sizes are needed for the microposts. However, it is an inexpensive approach to generate a master for PDMS stamps used in microcontact printing ECM proteins onto the tops of the microposts as described below (also in Chapter 19 by Lele *et al.*, this volume).

B. SU-8 Photolithography for Micropost Arrays

Currently, mPADs masters are made with SU-8 (MicroChem Corp., Newton, Massachusetts), which is a negative, epoxy-type, near-UV photoresist. Unlike common photoresists used as a protective layer for subsequent etching or deposition of materials, SU-8 has found widespread use in MEMS applications as a structural layer. Due to its high viscosity, SU-8 can be spun as thick as 2 mm and can achieve features with height-to-width aspect ratios as great as 25 with standard photoexposure systems. SU-8 is a highly functionalized molecule with eight epoxy groups (1,2-epoxide), where photogeneration of acid initiates cross-linking sites and renders it insoluble and mechanically rigid (4 GPa; Lorenz *et al.*, 1997). It is an

excellent material for making the mPADs master due to its ability to produce the high aspect ratio required for the microposts, its compatibility with standard exposure systems, and its mechanical strength for subsequent soft lithography.

The lithography of the mPADs master involves two lithography steps to create layers of SU-8 resist (Fig. 2). The first layer is unpatterned and UV exposed without a mask (flood exposure) to create a base for the microposts. The second layer is patterned with a dark-field chrome mask with arrays of $D = 3$-μm holes in the metal film, spaced $S = 9$-μm center-to-center to create the micropost arrays. The double layer of SU-8 ensures good adhesion between the posts and the underlying silicon wafer.

Before the first layer is spun on, the test grade, *n*-type, $\langle 100 \rangle$ silicon wafer (Silicon Quest International, Santa Clara, California) is dehydrated at 175°C for 30 min on a hot plate (Model 721A, Barnstead, Dubuque, Iowa) and ozone cleaned (Model 342, Jelight, Irvine, California) for 10 min to prime the wafer surface for optimal attachment of SU-8. SU-8 2002 is spun onto the wafer at 500 rpm for 5 sec followed by a ramp up to 2000 rpm for 30 sec to create a base layer of 2-μm thickness in a spin coater (WA400B-6NPP-LITE, Laurell, North Wales, Pennsylvania). The SU-8 film is soft baked at 65°C for 1 min and then 95°C for 2 min on a hot plate to dry the solvent out of the film. Next, the SU-8 film is exposed to UV light (365 nm) in an MJB-3 mask aligner (Karl Suss, Munich, Germany) without a photomask at 70 mJ of total light energy (=power × time). After the exposure, the wafer is postexposure baked with the same temperature conditions as the soft-baked step, in order to thermally drive the cross-linking reaction. The SU-8 film is then allowed to cool for 1 h at room temperature before spinning the next layer of photoresist.

For the second layer of SU-8, which will form the microposts, SU-8 2010 is spun at 500 rpm for 5 sec followed by a ramp up to 4000 rpm for 30 sec, yielding a 10-μm thick film. The film is soft baked with the same conditions as before. To pattern arrays of microposts, a dark-field photomask (Advanced Reproductions, North Andover, Massachusetts) is loaded into the MJB-3 mask aligner, placed into hard contact with the photoresist on the wafer, and exposed to 80 mJ of total light energy. The wafer is then postexposure baked with the same conditions as before to cross-link the pattern. Afterward, it is allowed to slowly cool to room temperature to reduce cracking in the SU-8 film.

To develop the pattern, the wafer is placed in a glass dish containing propylene glycol methyl ether acetate (PGMEA) to dissolve away the unexposed SU-8. (Note that PGMEA is an organic solvent and should be handled in a chemical fume hood.) After 2 min in the developer, the wafer is transferred to a second glass dish containing PGMEA for 5 sec to dilute away the dissolved SU-8. Next, the wafer is transferred into a third dish containing isopropyl alcohol (IPA) for 20 sec to dissolve the PGMEA. After IPA, the wafer is quickly transferred into the fourth and fifth dishes containing hexane for 5 sec each to remove the IPA. The wafer is removed from the last dish and rapidly dried with nitrogen. Hexane has a lower surface tension than IPA and helps reduce micropost collapse due to capillary

forces. The master is now fully fabricated and inspection under a metallurgical microscope should reveal arrays of microposts. Hard baking at 150°C for 20 h is encouraged to increase the mechanical strength of the master. Although these steps have been described in detail, results will vary depending on the equipment used. We strongly suggest that these process parameters be optimized according to specific facilities.

C. Soft Lithography

PDMS (Sylgard 184, Dow Corning, Midland, Michigan) is an optically clear, biologically inert, silicone rubber that closely matches the contour of a micro- or nanofabricated mold when cured. This material has been used to make inexpensive microfluidic devices (Duffy *et al.*, 1998), microlens (Chen *et al.*, 2004; Xia *et al.*, 1996), or stamps for microcontact printing (Tien and Chen, 2001; Xia and Whitesides, 1998; Chapter 19 by Lele *et al.*, this volume). Here, it is used to replicate the micropost structures in SU-8 through a double casting procedure. A negative mold is cast from the master to create an inverse of the mPADs, which are arrays of holes. The second casting into the negative mold results in the array of PDMS microposts on which cells can be seeded. The advantage of the double casting process is that one master can be used to create over several hundred PDMS micropost arrays for fabrication cost savings, which reduces variability between "identical" devices and provides a large supply of substrates.

PDMS is mixed at a 10:1 base polymer to curing agent ratio and allowed to degas for 1 h. The master is placed in an aluminum weight boat and PDMS is poured onto the master to form a layer ~1-cm thick. The polymer is rapidly cured in a 110°C convection oven for 10 min. The polymer is allowed to cool for 10 min before cutting away the aluminum boat and gently peeling the master out of the negative mold. This casting procedure is repeated in order to generate a large batch of negative masters for the second casting.

The surfaces of the negative molds need to be passivated with a fluorinated silane in order to prevent the liquid PDMS from permanently bonding to the PDMS negative mold during the second casting. First, the molds are placed in a plasma etcher (SPI Supplies, West Chester, Pennsylvania) for 2 min to activate the PDMS surface groups. Afterward, the molds are loaded into a desiccator and a few drops of (tridecafluoro-1,1,2,2-tetrahyrooctyl)-1-trichlorosilane (United Chemical Technologies, Bristol, Pennsylvania) are placed on a glass slide inside the desiccator. The chamber is evacuated overnight to allow the silane gas to diffuse over the negative molds and covalently bond to the PDMS surface groups. Extreme caution should be taken with trichlorosilanes as they readily react with water vapor to generate hydrochloric gas, which is toxic if inhaled.

After passivation, PDMS can be cast into the negative molds and released without permanent bonding. PDMS is mixed at a 10:1 ratio and degassed for 30 min. A thin layer of PDMS is applied to the negative mold and then a glass slide or cover glass pretreated in a plasma etcher is placed on top to sandwich the film.

The mold is placed into a 110°C oven and cured for 20 h to ensure maximum cross-linking of the PDMS polymer. The mPADs, bound to the top cover glass or slide, is then peeled away from the negative mold and the excess PDMS runoff is trimmed with a razor blade. Large batches of substrates can be prepared and stockpiled for multiple experiments.

D. Troubleshooting and Helpful Suggestions

In lithography of SU-8, it is essential to make sure that there is good contact between the mask and SU-8 film in order to generate sharply defined posts. Due to its viscosity, SU-8 has more edge beading than most other photoresists. The excess SU-8 beads at the edge of the wafer, which introduces topographic features on the wafer and prevents its intimate conformal contact with the mask. The gaps between the mask and wafer result in light diffraction and pattern loss. Spinning SU-8 at higher speeds assists in material removal at the wafer edge. Additionally, edge beading can be removed by spraying the edge of a spinning wafer with PGMEA in a syringe. Another common problem with SU-8 processing is enlarged feature dimensions at the top of the film, often called T-topping. We suggest using a UV filter (U-360, Hoya Optics, San Jose, California) to reduce the amount of deep UV light (<350 nm) transmitted to the film to reduce the T-topping effect. Finally, we strongly encourage the optimization of process conditions that we have detailed. Screening a range of lithography condition—exposure times, lamp intensities, hot plate temperatures, and baking times—will help identify the appropriate parameters to enable repeatable SU-8 fabrication success.

III. Characterization of Micropost Spring Constant

When using the mPADs as a force sensor, each tip deflection reports the local traction force and the relationship is proportional to the spring constant of a micropost. An estimate of the spring constant can be obtained through classical relationships describing beam bending, which closely matches small deflections of the microposts. We assume that microposts have uniform material properties and dimensions across the entire array so that equivalent deflections reflect equivalent forces. Calibration is, however, required to obtain empirically the spring constant of the posts against the deflection of a calibrated, pulled glass microneedle.

A. Beam-Bending Theory

A micropost can be regarded as a cantilever beam, fixed at one end and loaded with forces at the other end, undergoing pure bending and negligible shearing (Fig. 3A). From the theory of slender beam bending, the relationship between force, F, and tip displacement, x, for a cylindrical beam is given by

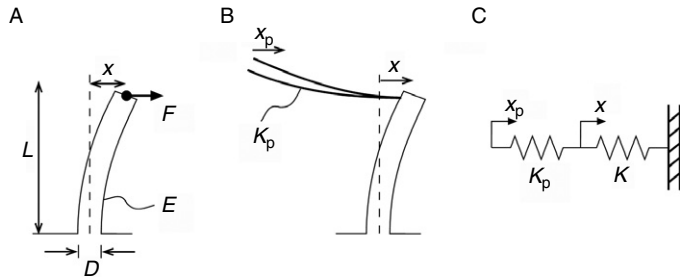

Fig. 3 Calculating the micropost stiffness. (A) Each micropost can be regarded as simple cantilever beam where the traction force, F, is linearly proportional to the tip deflection, x, as determined by the modulus of elasticity, E, the diameter, D, and height of the micropost, L. (B) Glass micropipettes can be used to empirically obtain the micropost stiffness by bring a calibrated tip with known stiffness, K_p, into contact with the posts and deflecting it by a known distance, x_p, while measuring the tip displacement of the post. (C) Equivalent two springs in series model used to calculate the micropost stiffness.

$$F = \frac{3\pi E D^4}{64 L^3} x \tag{1}$$

where E is the modulus of elasticity of PDMS (2.0–2.5 MPa), D is the diameter, and L is the height of the micropost. The diameter of the posts is measured optically with a calibrated microscope eyepiece reticle. The height is measured with a profilometer on the silicon master. The spring constant of the micropost is therefore $K = 3\pi E D^4/64L^3$. Calculation of this relationship provides the conversion from tip displacement (micrometers) to traction forces (nanonewtons) when cells are cultured on the array. A key assumption in the derivation of the spring constant equation is that vertical deflection of the micropost is small compared to horizontal deflection. For large tip deflections, a nonlinear relationship between force and deflection must be considered.

B. Measurement of Micropost Stiffness

The spring constant of the posts can be calibrated against the known spring constant of a glass micropipette prepared with a puller (World Precision Instruments, Sarasota, Florida). A crystal of *p*-nitrophenol was carefully placed on the end of the micropipette tip and the vertical deflection of the tip under the weight of the crystal (58 ± 32 μg) was recorded with a metallurgical microscope and measuring reticle. The microscope was horizontally mounted to observe the deflection of the tip. To determine the exact mass of the crystal, it was dissolved into bicarbonate buffer (50-mM Na_2CO_3, 50-mM $NaHCO_3$) and the transmittance of the solution at 400 nm was measured in a spectrophotometer (Lowry and Passonneau, 1972). The transmittance value was compared against a standard curve of transmission for known *p*-nitrophenol concentrations.

The calibrated micropipette can then be mounted on a micromanipulator and positioned into contact with a micropost, while under observation on an inverted phase microscope (Fig. 3B). The spring constant of the microposts can be found from the displacement of the micropost, x, against a prescribed translation of the micropipette, x_p, by the relationship for two springs in series,

$$K = \frac{K_p(x_p - x)}{x} \tag{2}$$

where K_p is the spring constant of the glass micropipette (Fig. 3C). We generally find close agreement between this direct measurement of K and calculated K as described above based on properties of PDMS and dimension of the posts.

IV. Analysis of Traction Forces Through Micropost Deflections

The mPADs are microcontact printed with ECM on the top surface to enable cells to attach and spread. This process involves the transfer of ECM proteins from a PDMS stamp to the tops of the microposts. The shaft and base are coated with a nonadhesive surfactant to confine cell attachment to the top. With proper coating, nearly all cell types are able to attach to the microposts and spread across the plane of tips. Spreading will be limited, of course, if the spacing S between posts becomes too large. For analysis of forces and identification of cellular structures responsible, the cells are fixed and immunofluorecently stained as one would do with cells on microscope cover glass. The samples are imaged in a fluorescent microscopy and images of the microposts are analyzed for deflections in MatLab (The Mathworks, Inc., Natick, Massachusetts).

A. Substrate Preparation

The methods of making and preparing micropatterned stamps for controlling cell adhesion area have been described elsewhere (Tan *et al.*, 2004; Tien and Chen, 2001; Chapter 19 by Lele *et al.*, this volume). Here, we discuss the general transfer of ECM onto the tops of all posts with a flat PDMS stamp (Fig. 4). First, PDMS and catalyst is mixed at a 30:1 ratio, allowed to degas, and then poured onto a silanized silicon wafer. The polymer is cured at 60°C for 1 h and then peeled from the wafer. The flat stamps are formed by cutting the PDMS into smaller pieces that match the mPAD array (typically 1×1 cm^2). In a biosafety cabinet, human fibronectin (BD Biosciences, San Jose, California) is prepared at 50 μg/ml in DI water. Aliquots of 50–100 μl are spread across the flat surface of the stamps and the protein is allowed to hydrophobically adsorb for 1 h to fully saturate the surface. Excess fibronectin is rinsed off in DI water and the stamp is dried with nitrogen. The PDMS surfaces of the mPADs are rendered hydrophilic with UV ozone treatment for 7 min in a UV Ozone cleaner (Jelight, Irvine, California). The flat

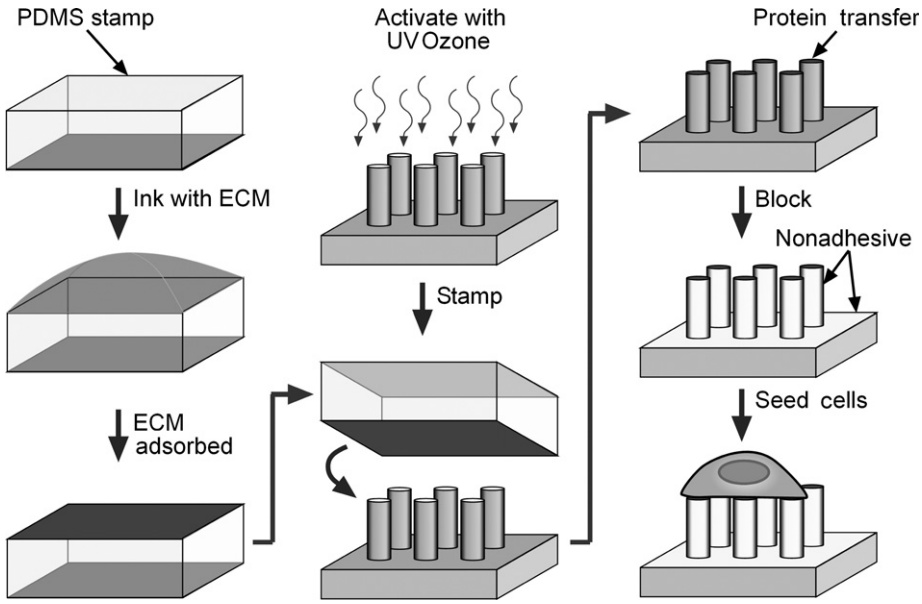

Fig. 4 Preparation of mPADs for seeding cells. ECM proteins are first applied to the top surface of a PDMS stamp by adsorption. Next, the mPADs are "activated" with UV ozone to change the PDMS surface from hydrophobic to hydrophilic, in order to allow transfer of proteins from the stamp to the tops of the microposts. The mPADs are then blocked with Pluronics to prevent nonspecific protein adsorption to unprinted areas. Finally, cells are seeded onto the microposts and allowed to spread for at least 10 h.

stamps are then placed over the microposts and pressed gently to form intimate contact with the microposts. The physical contact allows fibronectin to be transferred to the microposts by hydrophilic interactions.

After microcontact printing of the ECM protein, the mPADs undergo a series of sterilizing and washing steps. First, the mPADs are submerged in 100% ethanol to fully wet the microposts followed by 70% ethanol to sterilize the PDMS. The substrates are then washed in successive dishes containing DI water. The PDMS microposts are then stained with a lipophilic tracer (DiI, 1,1′-dioleyl-3,3,3′, 3′-tetramethylindocarbocyanine methanesulfonate, Invitrogen, Carlsbad, California) at 5 μg/ml for 1 h. The mPADs are washed with DI water and PBS to remove excess DiI and then submerged in 0.2% Pluronics F-127 (BASF, Ludwigshafen, Germany) for 30 min to prevent protein adsorption and cell adhesion to areas that were not stamped with ECM.

The substrates now have ECM on the tips and Pluronics blocking on the sides and base of the microposts. The mPADs are washed in successive dishes containing PBS and then placed into a standard tissue culture dish filled with the appropriate culture medium for the cell type. An mPADs substrate cast onto a standard $22 \times 22\ \text{mm}^2$ cover glass easily fits inside a 35-mm tissue culture dish. Cells are

harvested and seeded typically at a 1:10 ratio into the new dish using normal tissue culture procedures (Freshney, 2005). The seeding ratio affects the distance between cells and should be optimized to ensure a large likelihood of single cells for force analysis. After seeding, the mPADs are place in an incubator for at least 10 h to allow the cells to attach and spread on the microposts. The cells are then ready for experiments.

B. Staining and Microscopy of Micropost Arrays

Before microscopic imaging of the mPADs, the cells can be fixed and stained to identify specific structures, organelles, or proteins. We use 4% paraformeldahyde in PBS as our fixing solution to cross-link proteins, 0.05–0.2% Triton X-100 in PBS to permeabilize the membrane, and then antibodies or other fluorescent agents for immunofluorescent and direct staining. The samples can then be mounted onto a glass slide with a microscope cover glass overlaid on top for fluorescent and phase-contrast microscopy.

The first published technique for determining tip deflections compared a single fluorescent image of the grid deformed by traction forces, acquired at the focal plane of the tips of the posts, with an equally spaced grid that approximates the ideal, undeflected positions of the microposts (Tan *et al.*, 2003). The difference in positions, between the observed circular tops of the posts and the corresponding circles in the ideal grid, determined the magnitude and direction of tip deflection due to the traction forces.

We have since advanced the measurements by imaging the entire length of posts from top to base (Lemmon *et al.*, 2005). This method provides a more precise measure of micropost deflections because the base image of the posts approximates the undeflected position of the tips. It accurately shows any deviations in micropost position regularity due to defects in photomask design or microfabrication, which may be incorporated into the analysis for improved accuracy as described below. We use high-magnification objectives (60×) with oil to acquire our top and bottom images of the microposts.

C. Image Analysis Techniques

To calculate the direction and magnitude of the tip deflections, we use an image analysis routine developed with MatLab's image-processing toolbox (Lemmon *et al.*, 2005). The original code imports the acquired microscope images, performs a localized thresholding algorithm to calculate the centroids of the fluorescent microposts. This routine is repeated for both top and bottom images and generates respective matrices of centroid positions. The difference in positions (in pixels) between the top and bottom images is then converted to traction forces (nanonewtons) by converting pixel to micrometer and multiplying the displacement by the spring constant of the microposts. The calculated deflections can be used to generate vector plots of the resulting cell-generated forces. If MatLab is

not accessible, a similar imaging process can be implemented with other software programs such as IPLab (Scanalytics, Rockville, Maryland) or IGOR Pro (Wavemetrics, Lake Oswego, Oregon). We freely share our MatLab code on request.

V. Experimental Applications of Microposts and Discussion

On the mPADs, cells exert an average traction force per micropost on the order of tens of nanonewtons. Often, a range of three decades of traction forces (1–100 nN) is observed to be exerted by a cell attached to the posts, with largest forces at the perimeter and smallest ones in the interior. We consider the lower limit on force resolution to be equal to the variance in the apparent forces reported on the microposts that are not attached to cells and have no net force exerted on them. Using current techniques, this limit is ~3.2 nN.

One modification of the technique involves functionalizing only a subset of the microposts with ECM protein, in order to constrain cells to adhere to a specific geometry (square, rectangle, triangle, and so on) or total area (2×2 posts, 3×3 posts, and so on). In this case, instead of using a flat stamp, ECM can be loaded onto a stamp with microfeatures that have the desired printing dimensions and transferred to the tops of the microposts for patterning cells. This technique has been used to demonstrate that cell area positively correlates with average traction force per post (Tan *et al.*, 2003). In scaling up, larger stamp features may be used to produce patterned clusters of cells on the mPADs to study the cooperative effect of traction forces within a monolayer of cells (Nelson *et al.*, 2005).

The spring constant of the microposts can be adjusted by changing the height or diameter of the posts to measure the relationship between traction force generation and underlying substrate stiffness. In addition, while the procedure described above generates posts with a center-to-center distance $S = 9\ \mu$m, it can be used down to a resolution of $\sim 3\ \mu$m. Spatial resolution has been further increased by shortening S to 1.6, by the use of deep reactive ion etching (DRIE) to generate the high aspect ratio features (Du Roure *et al.*, 2005; Saez *et al.*, 2005). However, because DRIE is not as widely available and can be expensive, the cost-to-benefit ratio should be considered when deciding on which fabrication process to use. Through screening a range of aspect ratios of the posts, such variations in post geometry indicate that there is a strong correlation between substrate stiffness and traction force generation (Saez *et al.*, 2005). We have looked at traction forces with respect to cell types and have found that there is also phenotypic specificity in force generation for endothelial cells, epithelial cells, fibroblasts, and smooth muscle cells (Lemmon *et al.*, 2005).

Analysis of the spatiotemporal dynamics of traction forces is also permissible with the mPADs. A fluorescent microscope equipped with a chamber for regulating live cell conditions (temperature, CO_2, and humidity) can be employed to record the traction force over time during isometric contraction or directed migration of a cell. To analyze these images, a single bottom image is acquired and used as the reference

image for subsequent frames of the tip deflections in the top image. Attention should be made to accurately register the frames to the reference image because shifting in the sample position relative to the objective is common due to thermal fluctuations of the microscope or transmittance of vibration during operation. Additionally, one can fabricate mPADs onto a microscope cover glass and assemble them as the bottom of PDMS chambers for high-resolution measurements with oil immersion objectives.

It should be pointed out that the microposts provide a different topography to cells from the planar surface of glass or plastic tissue culture dishes. Such topography may introduce additional signals that could alter cell behavior, and requires further study. This possibility also raises the interesting question of whether flat surfaces or regularized discrete features are better models for the complex fibrous ECM that cells typically encounter *in vivo*. One important observation is that cells on mPADs appear qualitatively similar to those on glass coverslips in cell shape and organization of stress fibers and FAs, and generate similar traction forces as do cells cultured on flat polyacrylamide substrates (Lemmon *et al.*, 2005). Thus, while observations should always be checked by comparing different systems, these data suggest that the mPADs can provide meaningful insight into the mechanics of cultured cells.

Acknowledgments

The authors would like to thank John L. Tan and Michael T. Yang for their helpful discussions. This work was supported in part by the National Institutes of Health (grants EB00262 and HL073305), the Department of Defense Multidisciplinary University Research Initiative, DARPA, and the Nano/Bio Interface Center through the National Science Foundation NSEC DMR-0425780. NJS is supported by the National Institutes of Health Ruth Kirschstein National Research Service Award Postdoctoral Fellowship.

References

Adelstein, R. S. (1982). Calmodulin and the regulation of the actin-myosin interaction in smooth muscle and nonmuscle cells. *Cell* **30**(2), 349–350.

Balaban, N. Q., Schwarz, U. S., Riveline, D., Goichberg, P., Tzur, G., Sabanay, I., Mahalu, D., Safran, S., Bershadsky, A., Addadi, L., and Geiger, B. (2001). Force and focal adhesion assembly: A close relationship studied using elastic micropatterned substrates. *Nat. Cell Biol.* **3**(5), 466–472.

Brenner, B. (2006). The stroke size of myosins: A reevaluation. *J. Muscle Res. Cell Motil.* **27**(2), 173–187.

Campbell, S. A. (2001). "The Science and Engineering of Microelectronic Fabrication," 2nd edn., Vol. xiv, pp. 603. The Oxford series in electrical and computer engineering. Oxford University Press, New York.

Chen, J., Wang, W., Fang, L., and Varahramyan, K. (2004). Variable-focusing microlens with microfluidic chip. *J. Micromech. Microeng.* **14,** 675–680.

Chrzanowska-Wodnicka, M., and Burridge, K. (1996). Rho-stimulated contractility drives the formation of stress fibers and focal adhesions. *J. Cell Biol.* **133**(6), 1403–1415.

Dembo, M., and Wang, Y. L. (1999). Stresses at the cell-to-substrate interface during locomotion of fibroblasts. *Biophys. J.* **76**(4), 2307–2316.

Discher, D. E., Janmey, P., and Wang, Y. L. (2005). Tissue cells feel and respond to the stiffness of their substrate. *Science* **310**(5751), 1139–1143.

Duffy, D. C., McDonald, J. C., Schueller, O. J. A., and Whitesides, G. M. (1998). Rapid prototyping of microfluidic system in poly(dimethylsiloxane). *Anal. Chem.* **70**(23), 4974–4984.

Du Roure, O., Saez, A., Buguin, A., Austin, R. H., Chavrier, P., Siberzan, P., and Ladoux, B. (2005). Force mapping in epithelial cell migration. *Proc. Natl. Acad. Sci. USA* **102**(7), 2390–2395.

Finer, J. T., Simmons, R. M., and Spudich, J. A. (1994). Single myosin molecule mechanics: Piconewton forces and nanometre steps. *Nature* **368,** 113–119.

Freshney, R. I. (2005). "Culture of Animal Cells: A Manual of Basic Technique," 5th edn., p. 642. Wiley-Liss, Hoboken, NJ.

Galbraith, C. G., and Sheetz, M. P. (1997). A micromachined device provides a new bend on fibroblast traction forces. *Proc. Natl. Acad. Sci. USA* **94**(17), 9114–9118.

Geiger, B., Bershadsky, A., Pankov, R., and Yamada, K. M. (2001). Transmembrane extracellular matrix—cytoskeleton crosstalk. *Nat. Rev. Mol. Cell Biol.* **2**(11), 793–805.

Harris, A. K., Wild, P., and Stopak, D. (1980). Silicone rubber substrata: A new wrinkle in the study of cell locomotion. *Science* **208**(4440), 177–179.

Helfman, D. M., Levy, E. T., Berthier, C., Shtutman, M., Riveline, D., Grosheva, I., Lachish-Zalait, A., Elbaum, M., and Bershadsky, A. D. (1999). Caldesmon inhibits nonmuscle cell contractility and interferes with the formation of focal adhesions. *Mol. Biol. Cell* **10**(10), 3097–3112.

Huxley, H. E. (2004). Fifty years of muscle and the sliding filament hypothesis. *Eur. J. Biochem.* **271**(8), 1403–1415.

Ingber, D. E. (1993). Cellular tensegrity: Defining new rules of biological design that govern the cytoskeleton. *J. Cell Sci.* **104**(Pt. 3), 613–627.

Ingber, D. E. (2003). Tensegrity I. Cell structure and hierarchical systems biology. *J. Cell Sci.* **116**(Pt. 7), 1157–1173.

Jaeger, R. C. (2002)."Introduction to Microelectronic Fabrication," 2nd edn., Vol. xiv, p. 316. Prentice Hall, Upper Saddle River, NJ.

Lee, J., Leonard, M., Oliver, T., Ishihara, A., and Jacobson, K. (1994). Traction forces generated by locomoting keratocytes. *J. Cell Biol.* **127**(6 Pt. 2), 1957–1964.

Lemmon, C. A., Sniadecki, N. J., Alom Ruiz, S., Tan, J. T., Romer, L. H., and Chen, C. S. (2005). Shear force at the cell-matrix interface: Enhanced analysis for microfabricated post array detectors. *Mech. Chem. Biosyst.* **2**(1), 1–16.

Lorenz, H., Desont, M., Fahrni, N., LaBianca, N., Renaud, P., and Vettiger, P. (1997). SU-8: A low cost negative resist for MEMS. *J. Micromech. Microeng.* **7,** 121–124.

Lowry, O. H., and Passonneau, J. V. (1972)."A Flexible System of Enzymatic Analysis," Vol. xii, p. 291. Academic Press, New York.

Madou, M. J. (1997). "Fundamentals of Microfabrication," p. 589. CRC Press, Boca Raton, FL.

Nelson, C. M., Jean, R. P., Tan, J. L., Liu, W. F., Sniadecki, N. J., Spector, A. A., and Chen, C. S. (2005). Emergent patterns of growth controlled by multicellular form and mechanics. *Proc. Natl. Acad. Sci. USA* **102**(33), 11594–11599.

Saez, A., Buguin, A., Silberzan, P., and Ladoux, B. (2005). Is the mechanical activity of epithelial cells controlled by deformations or forces? *Biophys. J.* **89**(6), L52–L54.

Scholey, J. M., Brust-Mascher, I., and Mogilner, A. (2003). Cell division. *Nature* **422**(6933), 746–752.

Tan, J. L., Liu, W., Nelson, C. M., Raghavan, S., and Chen, C. S. (2004). Simple approach to micropattern cells on common culture substrates by tuning substrate wettability. *Tissue Eng.* **10**(5–6), 865–872.

Tan, J. L., Tien, J., Pirone, D. M., Gray, D. S., Bhadriraju, K., and Chen, C. S. (2003). Cells lying on a bed of microneedles: An approach to isolate mechanical force. *Proc. Natl. Acad. Sci. USA* **100**(4), 1484–1489.

Tien, J., and Chen, C. S. (2001). Microarrays of cells. *In* "Methods in Tissue Engineering" (A. Atala and R. Lanza, eds.), pp. 113–120. Academic Press, San Diego.

Xia, Y., Kim, E., Zhao, X. M., Rogers, J. A., Prentiss, M., and Whitesides, G. M. (1996). Complex optical surfaces formed by replica molding against elastomeric masters. *Science* **273**(5273), 347–349.

Xia, Y. N., and Whitesides, G. M. (1998). Soft lithography. *Angew. Chem. Int. Ed.* **37**(5), 551–575.